Part I

Intercalation Anodes for Advanced Lithium Batteries

HOST-GUEST SYSTEMS IN MICROPOROUS CARBONS

Toshiaki ENOKI*, Kazuyuki TAKAI*, Yoshiyuki SHIBAYAMA*, Norikazu KOBAYASHI*, Atsuko NAKAYAMA*, Hirohiko SATO*, Naohiko YOSHIDA**, Hidekazu TOUHARA**
*Department of Chemistry, Tokyo Institute of Technology, Ookayama, Meguro-ku, Tokyo 152-8551, Japan
**Department of Chemistry, Faculty of Textile Science and Technology, Shinshu University, Ueda 386-8567, Japan

ABSTRACT

Microporous activated carbon fibers (ACF) having huge specific surface areas are characterized as a three-dimensional network of nano-sized graphite domains. We investigate ACF-hosting host-guest systems aiming at novel phenomena produced by the host-guest interface interactions. An extraordinarily large amount of helium is condensed in the ACF micropores, suggesting the presence of ultra-micropores and the enhancement in the helium-nano-graphite interaction. Chemisorbed oxygen molecules are stabilized in the singlet states caused by the interaction with nano-graphite and it makes the micorpore volume swell. Iodine forms an intercalation system with nano-graphites through charge transfer process, in contrast with the behavior of bulk graphite that does not accept iodine as an acceptor-type intercalate. Fluorine reacting with nano-graphite generates dangling bond spins by breaking graphite π-bonds, where the fluorine-induced defect is found to have a widely extended electronic structure.

INTRODUCTION

Activated carbon fibers (ACF) are featured with a three-dimensional network of nano-sized graphites comprising the stacking of three to four graphene sheets with sizes of 2-3nm. The micropore space generated as the reversal of the nano-graphite network has huge specific surface areas ranging to 3000m^2/g which is available for the accommodation of guest species through intercalation or inclusion processes. In the micorpore space, guests are expected to form novel structural and electronic features in geometrically confined pore space with host-guest interaction. In addition, the host-guest interaction can happen to give interesting phenomena at the interface, which are not seen in the bulk systems. Therefore, the micropore is an important object with which novel classes of guest phases can be produced different from those in the ordinary bulk state. Especially, the pores surrounded by metallic nano-sized graphites having finite size π-electron systems are expected to provide additional characteristics to the features of the guest assemblies. Namely, the structures and electronic features of the guests are strongly affected by the charge transfer between nano-graphites and guests or the dielectric effect of the metallic graphitic planes.

Under the motivation mentioned above, we have been investigating the structures, electronic and magnetic properties of various guest species in the ACF micropores [1-10]. In this paper, we focus on helium, oxygen, fluorine and iodine as guest species in ACFs. Helium that is considered to be most inert is found to show an extraordinarily dense condensation in the micropores. Oxygen molecules lose their magnetism upon adsorption into ACFs due to the formation of singlet state and works to expand the inter-nano-graphite distances. In the case of iodine molecules, charge transfer takes place from nano-graphite to iodine resulting in the

Mat. Res. Soc. Symp. Proc. Vol. 548 © 1999 Materials Research Society

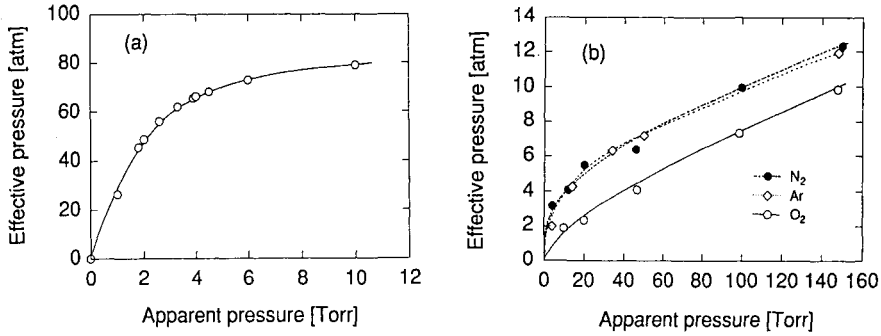

Fig.1. The effective pressure in the micropores as a function of apparent pressure at room temperature for (a) He, and (b) N_2, O_2 , and Ar. The solid, dashed and dot-dash lines are guide for the eyes.

formation of an intercalation compound, in contrast to the case of bulk graphite. The introduction of most chemically active fluorine brings about the formation of sp^3 defects having localized magnetic moments accompanied with local lattice distortion.

HUGE HELIUM GAS CONDENSATION

Figure 1 shows the adsorption isotherms of helium, nitrogen, argon, and oxygen gases at room temperature in pitch-based ACFs (Osaka Gas A30) having specific surface areas of $3000m^2/g$ [4]. It is revealed that the guest gaseous species are condensed in the micropores. In all cases except the helium adsorption, the condensation rates into the micropores, which are defined as the ratio of the effective pressure inside the pores to the pressure of the outside, range around 50-100 as exhibited in Fig.1(b). Figure 1(a) demonstrates exceptional behavior in the helium adsorption; that is, the condensation rate reaches almost 6000, which is about two orders of magnitudes larger than that in other gases. It is worth noting that the effective pressure of 80 atm at an outside pressure of 100 Torr is almost 1/10 of the pressure that helium gas possesses when liquid helium is converted to gas having the equivalent volume. Consequently, helium shows an extraordinarily huge condensation in the ACF micropores even at room temperature, though it is considered to be most inert gas in ordinary condition. The huge condensation is evidenced in the ESR investigation as well. Nano-graphites have localized spins around their peripheries that are suggested to originate from specific electronic structure of the nano-graphite edges according to a recent theoretical work [11]. The spin concentration is estimated at ca.10^{19}/g from ESR investigation [1,6]. Accordingly, the localized spins are employed as a probe to detect the effect of helium atoms accommodated in the micropores. In the present work, the spin-lattice relaxation mechanism is investigated using the ESR saturation technique in order to make clear the interaction between helium atoms and the localized spins on nano-graphites. Figure 2 shows the ESR saturation curves for the ACF sample in vacuum and under the presence of 10 Torr helium, argon, nitrogen, and oxygen. The saturation curves for hydrogen and neon are almost identical to the curve for nitrogen or argon. The localized spins of ACFs in vacuum gives a trend of rather easy saturation in the low microwave power range. This means that the phonon-assisted spin-lattice relaxation process, which is know to govern in ordinary bulk graphite, is not effective due to the finite size effect of nano-graphites on the phonon spectrum, resulting in the deceleration of the spin-lattice relaxation rate. From the saturation

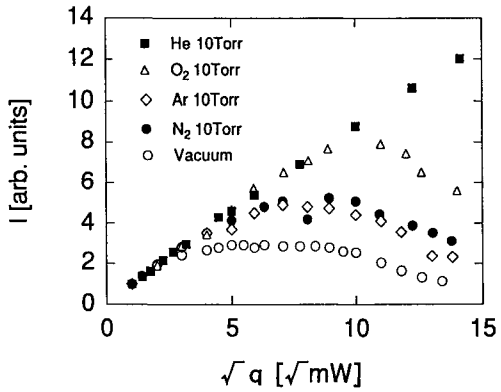

Fig.2. The microwave power (q) dependence of the ESR intensity (I) under the presence of gaseous materials; He, N_2, O_2 and Ar. The behavior of the sample with H_2 or Ne is almost identical to that with N_2 or Ar.

curve, the spin-lattice relaxation rate is estimated at $1/T_1 \approx 10^5$ sec^{-1} for ACFs in vacuum. When foreign guest gases are introduced, the saturation curves becomes less saturated irrespective of the differences in internal degrees of freedom and masses of guest molecules. This proves an important participation of accommodated guest species in the spin-lattice relaxation mechanism. The behavior of the saturation curves is almost same among hydrogen, nitrogen, neon, and argon molecules, which prefer the surfaces of graphene sheets as adsorption sites [12]. Oxygen molecules show a different trend in the saturation curve that is roughly featured with a homogeneous spin system [4, 10]. This suggests that adsorbed oxygen molecules as discussed later prefer chemically active edge sites around the nano-graphite peripheries. Interestingly, in the case of helium adsorption, Fig.2 reveals the absence of saturation behavior in the microwave power range investigated, suggesting a large acceleration of the spin-lattice relaxation rate. The estimated spin-lattice relaxation rate becomes more than one order of magnitude larger even in 10 Torr of helium gas than that of ACFs in vacuum. In other words, the increase in the pressure of helium gas is found to enhance the rate strongly. As a consequence, the collisions of molecules to the localized spins are considered to govern the spin-lattice relaxation process, taking into account that the phonon-assisted process otherwise effective is ruled out in the present case. Moreover, the extremely large condensation of helium works most effectively in the collision-assisted spin-lattice relaxation process.

Here, we discuss the mechanism of the helium-atom-collision-assisted spin-lattice relaxation [5]. Around the periphery of a nano-graphite domain, there are edge-electronic states having localized spins that interact with π-electron conduction carriers. When a helium atom approaches an electron at the edge state, the van der Waals interaction works between them, whose origin is ascribed to the electric dipole-dipole interaction. The spin-lattice relaxation rate $1/T_1$ is described in the following equation;

$$1/T_1 = n v \sigma, \qquad (1)$$

where n,v and σ are the density of helium atoms, the mean velocity of the helium atom, and the cross section of a helium collision related to the dipole-dipole interaction and the spin reversal process, respectively. The spin-lattice relaxation process takes place with assistance of the spin-orbit interaction in the nano-graphite π-electrons. Using Eq.(1) with the detailed information on

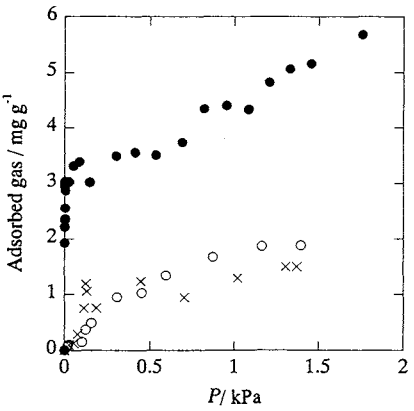

Fig.3. Adsorption isotherms for oxygen and nitrogen at 298K. Full circles denote the oxygen adsorption on a fresh ACF sample while crosses show the oxygen adsorption on the sample that has been evacuated at room temperature after the first oxygen adsorption. Open circles are for the nitrogen adsorption.

the electronic states of the π-electrons and the helium electrons [5], the spin-lattice relaxation rate is calculated at $1/T_1 \approx 10^6$ sec^{-1}, which is in good agreement with that observed in the experiment. Eventually, the ESR experiment gives a supplemental evidence of the huge condensation of helium in the micropore space.

Here still remains a problem concerning the reason why only helium atoms are condensed in an exceptionally large amount. Kaneko et al. suggest the presence of ultra-micropores which can accommodate only small diameter helium atoms in ACFs [13]. In addition to this, it is known that the interaction between a helium atom and an ion is enhanced more than two orders of magnitude in comparison with that for a neutral atom which is in the range of ~1K [14]. This indicates that the novel electronic state of nano-graphite edges plausibly enhances the interaction between helium atoms and nano-graphites, resulting in the huge helium condensation in the ACF micropores.

OXYGEN ADSORPTION

The adsorption of oxygen molecules has a different trend from that of helium or other gases investigated in the preceding section, a part of which is seen in Figs.1 and 2. In this section, we discuss the novel adsorption state of oxygen molecules on the basis of phenol-based ACFs (Kurare FR20) having specific surface areas of $2000m^2/g$. Figure 3 shows the adsorption isotherms of oxygen taken at room temperature, which is compared with that of nitrogen. The adsorption isotherm of a fresh ACF sample just after the vacuum-heat-treatment at 200℃ shows a steep increase in the low pressure range, followed by a subsequent linear increase with the pressure increase. In the meantime, the adsorption isotherm after the evacuation of the sample at room temperature used in the first run has no initial steep increase, which behaves almost similarly to that of nitrogen adsorption. Therefore, there are two types of adsorption sites; that is, the steep initial slope corresponds to strong adsorption sites, while the subsequent linear change originates from weak physisorption sites. The concentration of strong adsorption sites is estimated at $6\times10^{19}/g$, which is comparable to the concentration of localized spins of

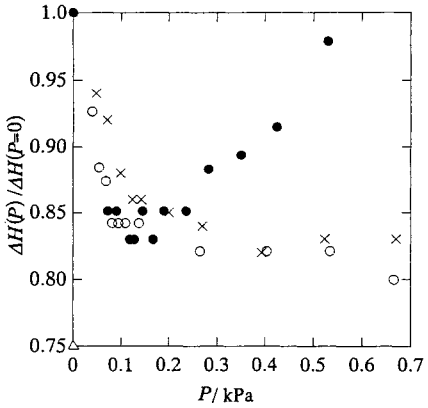

Fig.4. Pressure dependence of the ESR line width after the introduction of oxygen (full circle), nitrogen (open circle) and helium (cross) for the fresh ACF sample at room temperature. The line width is normalized with the line width ΔH~5mT of the sample before gas uptake. The open triangle at P=0kPa corresponds to the line width observed for the sample evacuated at room temperature after the oxygen adsorption experiment. The subsequent heat-treatment in vacuum at 473K makes the line width recovered to the initial value (ΔH~5mT).

nano-graphite edge origin (3×10^{19}/g). As the spin concentration corresponds to ~one spin/nano-graphite on average [8], it is suggested that there is about one strong adsorption site per nano-graphite. The ESR saturation curve shown in Fig.2 reveals different feature from the saturation curves of other gaseous species investigated. This can be explained by the presence of strong adsorption sites for oxygen molecules, which are not available for the other gases such as nitrogen. Taking into account the structure of a nano-graphite consisting of three to four graphene sheets, the edges of graphene sheets are considered to contribute to adsorption sites that are chemically active due to the presence of functional groups, as well as the surfaces of graphene sheets. Consequently, the strong adsorption sites accommodating only chemically active oxygen molecules are ascribed to the edges of graphene sheets, while the graphene surfaces work as weak physisorption sites, which accept all kinds of guest species.

The oxygen species accommodated in the strong adsorption sites have anomalous features, which ordinary gaseous oxygen molecules do not have. Figure 4 shows the ESR line width of the localized spins of ACFs taken at room temperature under the atmosphere of oxygen, nitrogen and helium gases. The ESR line width, whose value is about 5mT for the sample before gas uptake, decreases upon gas uptake irrespective of introduced gas species in the low pressure range up to 0.1kPa where oxygen molecules occupy completely the strong adsorption sites (chemisorption sites). The decrement at 0.1kPa is estimated at 15-17% for all the guest gas species. In the higher-pressure range in which physisorption becomes predominant, no pressure dependence is observed for nitrogen and helium, while oxygen that is magnetically active due to the triplet state shows a linear increase above 0.1kPa. The raising trend in oxygen gas can be explained in terms of the dipole-dipole interaction between the localized spin and the oxygen spin. The increase in the oxygen concentration enhances the interaction resulting in the increase in the line width.

The origin of the decrease in the line width in the low pressure range is clarified in

connection with the electrical conductivity change in ACFs upon gas uptake. The electron conduction mechanism is explained by the hopping process of an electron between nano-graphite islands. When guest gas is introduced into the micropores of ACFs, the conductivity is lowered in the low-pressure range. The decrements of the conductivity are estimated at 13-15% at 0.1kPa for oxygen and nitrogen gases. An electron hopping event between nano-graphites is considered to be proportional to the overlap of the wave functions of the adjacent nano-graphites that is related to $\exp(-r/\xi)$ where r and ξ are the inter-nano-graphite distance and the extension of the wave function, respectively. Thus, the decrease in the conductivity is associated with the increase in the inter-nano-graphite distances. The decrease in the ESR line width gives complementary evidence for the increase in the inter-nano-garaphite distance. Taking into account that even chemically inactive nitrogen or helium works to generate the change in the ESR line width, the change should be ascribed not to the change in the electronic state of ACFs but to that of the structure. As the ESR signal has the feature of an inhomogeneous spin system, the line width is associated mainly with the dipole-dipole interaction between localized spins, where the interaction is inversely proportional to the cube of the inter-spin distance. Therefore, the change in the inter-spin distance gives a change in the line width. Judging from the fact that each nano-graphite has ca.1 spin on average, the decrease in the line width is explained by the increase in the distances between nano-gaphites. The calculation of the second moment for the line width gives an estimate of the increment of the inter-spin distance ~0.1nm. Eventually, the experimental results demonstrate that gas uptake makes the volume of micropores swell.

Next, we discuss the electronic state of the chemisorbed oxygen molecules in the micropores. There is no difference in the ESR line width between non-magnetic nitrogen and magnetic oxygen molecules in the low-pressure range, in contradiction to the expectation on the basis of the dipole-dipole interaction with magnetic oxygen molecules. The magnetic susceptibility of ACFs does not show any change when oxygen molecules are introduced into the micropores unless the oxygen concentration exceeds the concentration of the strong adsorption sites. This means that the oxygen molecules adsorbed on the strong adsorption sites are stablized in the singlet state, resulting in losing their magnetic feature. Consequently, oxygen molecules adsorbed in the micropore are found to have a novel electronic state, which is produced only under the influence of the ACF electronic system.

CHARGE TRANSFER BETWEEN NANOGRAPHITE AND IODINE GUEST

It is well known that polycyclic aromatic hydrocarbons such as perylene react with iodine resulting in the formation of charge transfer complexes [15], whereas graphite that is the extreme of polycylic aromatic hydrocarbons with an infinite size does not form any complex with iodine or in other words no graphite-iodine intercalation compound is produced. Accordingly, it is interesting to investigate the feature of interaction between iodine and nano-graphite, since nano-graphite is situated in between. We investigate the structure and electronic properties of ACF-iodine system using pitch-based ACFs (Osaka Gas A15) with specific surface areas of 1500m^2/g.

Figure 5 shows the heat-treatment temperature dependence of the nano-graphite mean in-plane sizes in ACFs in the temperature range up to 2800℃. The mean in-plane size of a nano-graphite is estimated at around 3nm for the non-heat-treated ACFs. It is independent of the heat-treatment temperature up to about 1000 to 1200℃, and then, above that temperature, it increases as the heat-treatment temperature is elevated. Such heat-treatment temperature dependence of the nano-graphite size is explained by the change in the structural features of ACFs. Namely, the

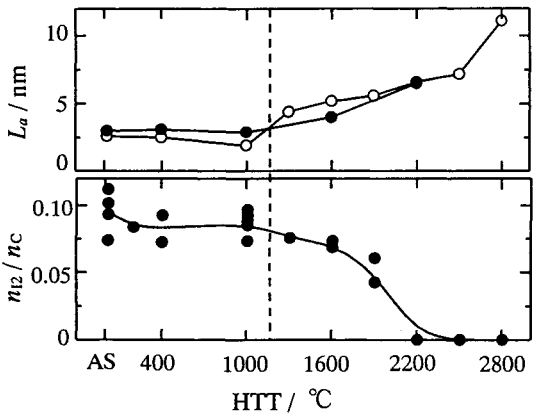

Fig.5. The heat-treatment temperature (HTT) dependence of the mean in-plane size of nano-graphites for the iodine-doped (full circle) and non-doped (open circle) ACFs (upper panel). The HTT dependence of iodine concentration n_{I2}/n_C in ACFs (lower panel). The dashed line denotes the metal-insulator boundary.

heat-treatment process in the low temperature range up to 900℃ induces stripping functional groups attached to the peripheral regions of nano-graphites, while graphitization takes place at high temperatures above 1600℃. The electronic properties are well correlated to the heat-treatment-induced change in the structures. In the low heat-treatment temperature range below 1000-1200℃, where nano-graphite domains are apart from each other, the electron conduction process in the nano-graphite network obeys Coulomb-gap variable-range-hopping conduction. The increase in the nano-graphite sizes above the heat-treatment temperature of 1000-1200℃ makes the inter-domain distances reduced to a threshold value at which the percolation paths of electrons are generated for metallic electron conduction in the nano-graphite network. Therefore, there exists a metal-insulator transition at a heat-treatment temperature 1000-1200 ℃ corresponding to the temperature of the threshold. The vertical dashed line in Fig.5 denotes the temperature of the percolation threshold, above which metallic conduction paths are completed. From the aspect of iodine uptake, the increase of the nano-graphite sizes taking place at the expense of specific surface areas brings about the shrinkage of the room that accommodates iodine guests. Figure 5 suggests this trend. The iodine concentration is estimated at n_{I2}/n_C~0.08 for the non-heat-treated ACF sample, which corresponds to ca.80 iodine atoms/nano-graphite. The iodine concentration is lowered as the elevation of the heat-treatment temperature. Especially, above 1600℃, the iodine concentration is steeply diminished, and finally, it becomes negligible at around 2200℃. It should be noted that iodine can be accommodated even around 1600℃ that is the temperature above which graphitization process takes place. Moreover, even around the heat-treatment temperature of the percolation threshold, each nano-graphite has ~10^2 iodine atoms.

Here, we discuss the interaction between the iodine species and nano-graphites on the basis of the electrical conductivity, thermoelectric powers and magnetic susceptibility. As mentioned above, the electronic features are characterized with the existence of a metal-insulator transition depending on the heat-treatment temperature. Therefore, the electronic structures are discussed differently between the insulating state and the metallic state. In the insulating state, the conductivity σ is explained in terms of the Coulomb-gap variable range

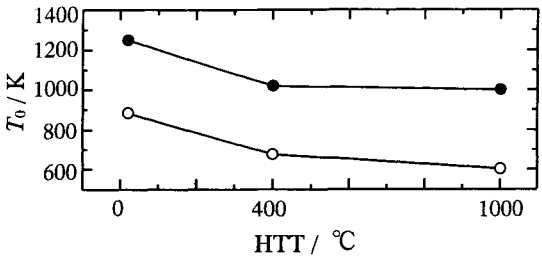

Fig.6. The heat-treatment temperature (HTT) dependence of T_0 for the iodine-doped (open circle) and non-doped (full circle) ACFs.

hopping mechanism, which is expressed in the following equation;

$$\sigma = \sigma_0 \exp\left[-(T_0/T)^{1/2}\right], \tag{2}$$

$$T_0 = \frac{3e^2}{2\pi^2 k_B \varepsilon \alpha^{-1}}, \tag{3}$$

where ε and α^{-1} are the dielectric constant of the medium surrounding nano-graphites and the localization length of the wave function, respectively. The values of T_0 are shown as a function of heat-treatment temperature in Fig. 6 for the iodine-doped and non-doped ACFs. The decrease in T_0 upon the heat-treatment is explained by the elimination of functional groups attached around the peripheries of nano-graphite domains by the heat-treatment, which makes the inter-domain-interaction enhanced. T_0 becomes reduced upon iodine doping for all the samples heat-treated at various temperatures up to 1000℃. This means that the accommodated iodine species in the micropores work to increase the dielectric constant. Moreover, the behavior of the orbital diamagnetic susceptibility, which reflects the electronic structure of the graphitic π-electron system, is not changed from that of the non-heat-treated ACFs, by the heat-treatment in that temperature range. As a consequence, the experimental finding proves that iodine species are simply accommodated in the micropore space without any electronic interaction with nano-graphite in the insulating region. The electronic structure in the metallic state is differently featured according to the behavior of the magnetic susceptibility and thermoelectric powers. The orbital diamagnetic susceptibility of π-electrons on nano-graphites is sensitive not only to the size of nano-graphite but also to the interaction with guests. The Fermi energy E_F related to the charge transfer from nano-graphite to the iodine can be estimated from the susceptibility [9]. The Fermi energy is lowered as the heat-treatment temperature is elevated both for the iodine-doped and non-doped ACFs. In nano-graphite, there exist hole carriers in the π-band generated by the interaction between the π-band and the non-bonding edge states, which are evidenced by the positive thermoelectric power [16]. The heat-treatment above 1200℃ makes the size of nano-graphite increase, resulting in the reduction in relative importance of the edges. Accordingly, the concentration of hole carriers decreases as the heat-treatment temperature is raised. The increase in the Fermi energy upon iodine doping is important evidence that electrons are transferred from the graphite π-band to iodine. The charge transfer rate f_c estimated from the Fermi energy is shown in Fig.7, where f_c is defined as the charge per carbon atom after the charge transfer from graphite to iodine. f_c is estimated at 0.009 at a heat-treatment temperature of 1300℃, which is just above the metal-insulator transition temperature. It decreases steeply